Proceedings of the ASME 2018 International Design Engineering Technical Conferences and Computers and Information in Engineering Conference IDETC/CIE 2018

August 26-29, 2018, Quebec City, Quebec, Canada

DETC2018-85932

USING MULTI-STABLE ORIGAMI MECHANISM FOR PERISTALTIC GAIT GENERATION: A CASE STUDY

Priyanka Bhovad* and Suyi Li
Department of Mechanical Engineering
Clemson University
Clemson, SC, USA

ABSTRACT

This study proposes and examines a novel approach to generate peristaltic locomotion gait in a segmented origami robot. Specifically, we demonstrate how to harness elastic multi-stability embedded in a soft origami skeleton to create an earthworm-like locomotion. Origami is attractive for building soft robots because it can exhibit the essential compliance and reduce the part count. Most importantly, it can work as an actuation mechanism. Moreover, embedding multi-stability into an origami skeleton allows it to remain in any of the stable states and switch between different states via a series of jumps. In this paper, we use two serially connected bistable Kresling segments, each featuring a generalized crease pattern design and a foldable anchoring mechanism, to develop a driving module for crawling soft robot. Multi-stability analysis of this dual-segment module reveals a four-phase actuation cycle, which is then used to generate the peristaltic gait. Instead of controlling the segment deformations individually like in earthworm and other crawling robots; we only control the total length of our driving module. This approach can significantly reduce the total number of actuators needed for locomotion and simplify the control requirements. The purpose of this paper is to combine the best features of multistable mechanisms and origami to advance the state of art of earthworm inspired crawling soft robot. Our results demonstrate the potential of using multi-stable origami mechanisms to generate locomotion gaits without the need of complex controllers.

1. INTRODUCTION

In recent years, the field of soft robotics has grown significantly and we are closer than ever to building truly soft machines that can collaborate with humans in various scenarios [1,2]. One important challenge of this field is to create soft robots capable of navigating with ease in a constrained working environment and with minimal hazard to people and/or objects nearby. To this end, researchers have successfully developed a wide variety of biomimetic soft robots capable of crawling, hopping, climbing, rolling, walking, swimming, etc. [1,2]. In this work, we focus on the gait generation for crawling soft robots mimicking a major mode of limbless terrestrial locomotion, namely *peristalsis*.

Peristaltic locomotion is observed in many soft segmented invertebrates, such as earthworms, for movement in different terrains [3]. The metameric segmentation of an earthworm coupled with the unique musculature allows each segment to deform independently and swiftly to generate locomotion gaits suitable for different conditions such as burrowing through soil, crawling on uneven surface, and climbing steep angles. These segments can be categorized as contracting, anchoring and extending [4]. Together they constitute a "driving module" for generating the peristaltic gait. The number and type of segments participating in each driving module can be varied to adapt to the local terrain.

Let's consider an example of earthworm peristalsis locomotion (Figure 1). In this example, the earthworm body has three driving modules, each consisting of two contracting, anchoring and extending segments. There are two unactuated segments between adjacent modules. An actuation cycle of peristalsis can be split into multiple phases of actuation period Δt . A cycle of peristalsis is then defined as time required for the earthworm to return to the first phase. The *gait length* is defined as the distance travelled by the earthworm during one cycle of peristalsis [3]. During an actuation phase (e.g. from t_0 to $t_0 + \Delta t$), contracting

^{*}Address all correspondence to this author: pbhovad@clemson.edu

segments deform to fully-contracted shapes (i.e. minimum length) and become anchoring segments. Similarly, extending segments deform to fully-extended shapes (i.e. maximum length) and become unactuated segments. By the end of the actuation phase (i.e. at $t = t_0 + \Delta t$), the anchoring segments become extending segments and the unactuated segments become contracting segments. These deformations are achieved by engaging the circular and longitudinal muscles within each segment [3]. The two muscle groups work antagonistically: contracting the circular muscles decreases segment diameter and increases its length, while contracting the longitudinal muscles increases segment diameter and reduces its length. The fully-contracted segments use external claw-like bristles on the body called 'setae' to anchor themselves to the environment. This (temporary) anchoring helps to produce forward movement; while the peristaltic wave travels in the opposite direction (Figure 1). At the end of each actuation phase, the driving modules move in the opposite direction of earthworm locomotion direction. Thus, the coordinated morphing of metameric segments in driving module generates wave-like locomotion gait called the 'peristalsis'.

Peristalsis is very well suited for building soft robots capable of moving through confined spaces because this locomotion mechanism does not require complex external appendages like legs or wheels. For example, a well-designed earthworm-like robot can burrow through rubble for disaster relief. Moreover, the individual segments used in the peristaltic locomotion serve as both skeletal structure and actuation mechanism. This approach can reduce structural complexity and decrease the overall mass of soft robot. Due to these potential advantages, there have been many studies to build soft crawling robots that can imitate the peristaltic locomotion [5–9].

A key challenge in the development of these soft robots is the design of kinematic and actuation mechanisms that can effectively and efficiently create the retrograde peristalsis wave (aka. locomotion gait) to move the robot forward. Gait generation schemes and driving actuators among these robots are vastly different, such as inflating and deflating pneumatic channels[5], SMA coil actuator mesh [6], SMA spring actuated origami structure [7], magnetic fluid filled segments [8] and servo actuator driven compliant modular mesh [9]. While these locomotion mechanisms could successfully generate the peristalsis gait, many of them require complex control architecture and highpower electromechanical actuators. For example, the slow actuation speed of SMA actuators and bulky pressurization control systems for pneumatic mechanisms are still some of the unaddressed challenges limiting the viability and portability of soft robots.

In this paper, we will elucidate a novel concept of directly exploiting the multi-stability embedded in an origami skeleton to generate peristaltic locomotion gait without the need of complicated actuation mechanisms or controllers. *Multi-stability* of a structure or a material system is a property of exhibiting more than one stable equilibria (or states), which can be characterized as the potential energy minima within the deformation range. A

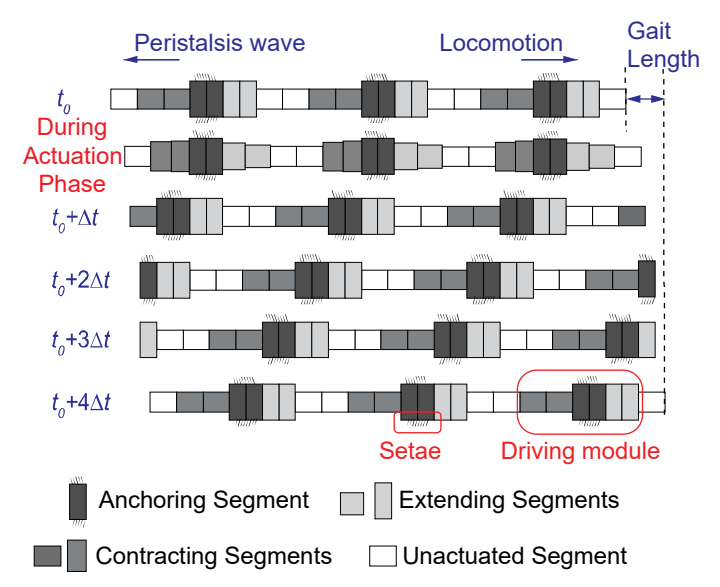


Figure 1: The concept of peristaltic locomotion. The driving module consists of contracting, (temporarily) anchoring, and extending segments. The earthworm body moves forward while the peristalsis wave travels backward. Δt denotes the actuation period.

multi-stable system can remain at any of the stable equilibria and switch between different states via rapid jump (or snap-through) actions. Therefore, by a careful application of external loads, one can switch the system between its different stable states in a predictable way.

Originally a recreational art; *origami* has attracted a lot of attention from scientific community in recent years. As opposed to traditional mechanisms with rigid linkages connected by moveable joints, an origami mechanism consists of a flat sheet folded at the pre-defined creases resulting in an intricate 3-D geometry. It imparts compliance to the soft robot without compromising on the structural strength. Therefore, using an origami unit for a soft robot skeleton can reduce the part count and complexity [10–14], while imparting unique capabilities such as self-packaging, multi-functional metamorphosis [15], and reduced power requirements [8,9]. Additionally, the scale-independent nature of origami signifies that we could create robots ranging from macro-scale to micro-scale using the same basic principles.

An earthworm like crawling robot segment ideally requires a tubular cross-section and an ability to produce large length changes (Figure 1). In particular, we are looking for bistable origami units that are elastically stable at both, fully-extended and fully-contracted shape. We found that the Kresling pattern based cylindrical origami satisfies these requirements. The robotic skeleton based on Kresling can be lightweight and soft yet structurally robust. Most importantly, multiple Kresling segments connected together can constitute a multi-stable driving module, which can be used for peristaltic gait generation. These properties make a Kresling segment very attractive candidate for building a crawling soft robot. To the best of our knowledge, this is

the first work to directly use the multi-stability concept to generate peristaltic locomotion gait.

The remaining parts of this paper are organized as follows. In section 2, we discuss the design of a *generalized bistable Kresling* segment which allows the user to freely prescribe its length at two different stable states to meet the different locomotion requirements. In section 3, we derive the formulation to analyze the multi-stable characteristics of a driving module consisting of multiple bistable segments. We use this formulation to perform the multi-stability analysis of Kresling based driving module. In section 4, we describe the peristaltic locomotion gait generation based on the results obtained from section 3. We conclude by summarizing the main findings in section 5.

2. DESIGN OF GENERALIZED KRESLING SEGMENT

The Kresling pattern was first investigated by Biruta Kresling [16] and a similar pattern was extensively studied by Guest and Pellegrino as well [17]. The geometric design and bistability of 'traditional' Kresling pattern has been discussed in depth in many studies [13,18,19]. The traditional Kresling pattern is designed as a flat-foldable mechanism, that is, its length at fully-folded stable state is exactly zero. Here, we propose and describe a 'generalized' Kresling pattern that can be tailored to feature a non-zero length at fully-folded state. This opens up new design spaces of Kresling pattern and can in particular accommodate the thickness of realistic sheet materials.

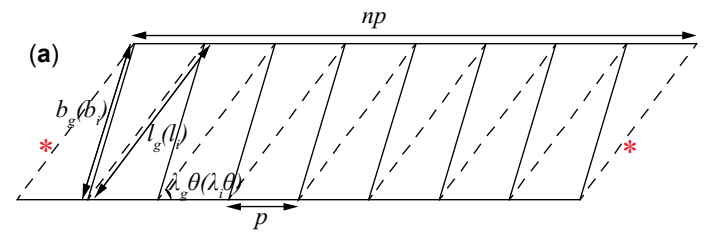
The design parameters of the generalized Kresling pattern are: n (number of sides of the base and top polygon), p (side length of the base and top polygon), λ_i (angle ratio), and L_{fc} (Kresling segment length at the fully-folded stable state). The corresponding crease pattern consists of equally spaced mountain and valley creases as shown in Figure 2(a). The first and last valley creases are glued together to generate a rotationally symmetric twisted polygonal prism. The base and top of the cylinder create regular polygons which are assumed rigid during the folding motion. To design the generalized Kresling pattern, we start from the traditional Kresling, with its geometry given by,

$$\phi = \frac{\pi}{n}; R = \frac{p}{2\sin\phi}; \theta = \frac{\pi}{2} - \phi, \tag{1}$$

$$l_i = 2R\cos(\theta - \lambda\theta),$$

$$b_i = (a^2 + l_i^2 - 2al_i\cos(\lambda\theta))^{1/2},$$
(2)

where ϕ is half the internal angle of the base and top polygon, R is the radius of the base and top polygon, θ is the angle between the radius vector and polygon side as shown in Figure 2(b). The top polygon of traditional Kresling segment is translated away from the bottom polygon by a distance of L_{fc} to create the generalized Kresling. The resulting crease pattern is no longer flatfoldable; but retains an identical range of rotation as viewed from the top. The new lengths of mountain and valley crease and the angle of inclination of valley crease are given by,



Mountain Crease- - - Valley Crease

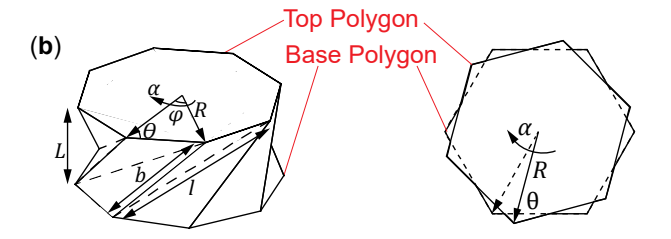


Figure 2: Generalized Kresling pattern (a) Crease pattern depicting the design parameters. The creases marked with (*) are glued together to create a Kresling segment. The geometric parameters for traditional Kresling are shown in brackets, (b) Isometric view and Top view of folded Kresling segment depict the important geometric parameters and the sign convention for angle of rotation α .

$$b_{g} = (b_{i}^{2} + L_{fc}^{2})^{1/2},$$

$$l_{g} = (l_{i}^{2} + L_{fc}^{2})^{1/2},$$

$$\lambda_{g} \theta = \cos^{-1}((p^{2} + l_{g}^{2} - b_{g}^{2})/(2pl_{g})).$$
(3)

Here, the subscript i refers to the parameters for traditional Kresling and subscript g refers to those for generalized pattern. The fully-folded length (L_{fc}) of the segment is set as per the user requirement. The angle of rotation (α) is used to characterize the unfolding and folding motion of a segment. The vertices of Kresling segment can be written in cylindrical co-ordinate system (R, α, L) and the lengths of mountain (b) and valley (l) crease calculated,

$$b = (2R^{2}(1-\cos(\alpha)) + L^{2})^{1/2},$$

$$l = (2R^{2}(1-\cos(\alpha+2\phi)) + L^{2})^{1/2}.$$
(4)

We use equivalent truss-frame approach to analyze the mechanics of generalized Kresling segment folding [19]. It can be assumed that the length of the diagonal crease (l) remains constant and only mountain crease (b) is compressed throughout the folding motion [17]. With this assumption, the derivative of l w.r.t. α is zero so that,

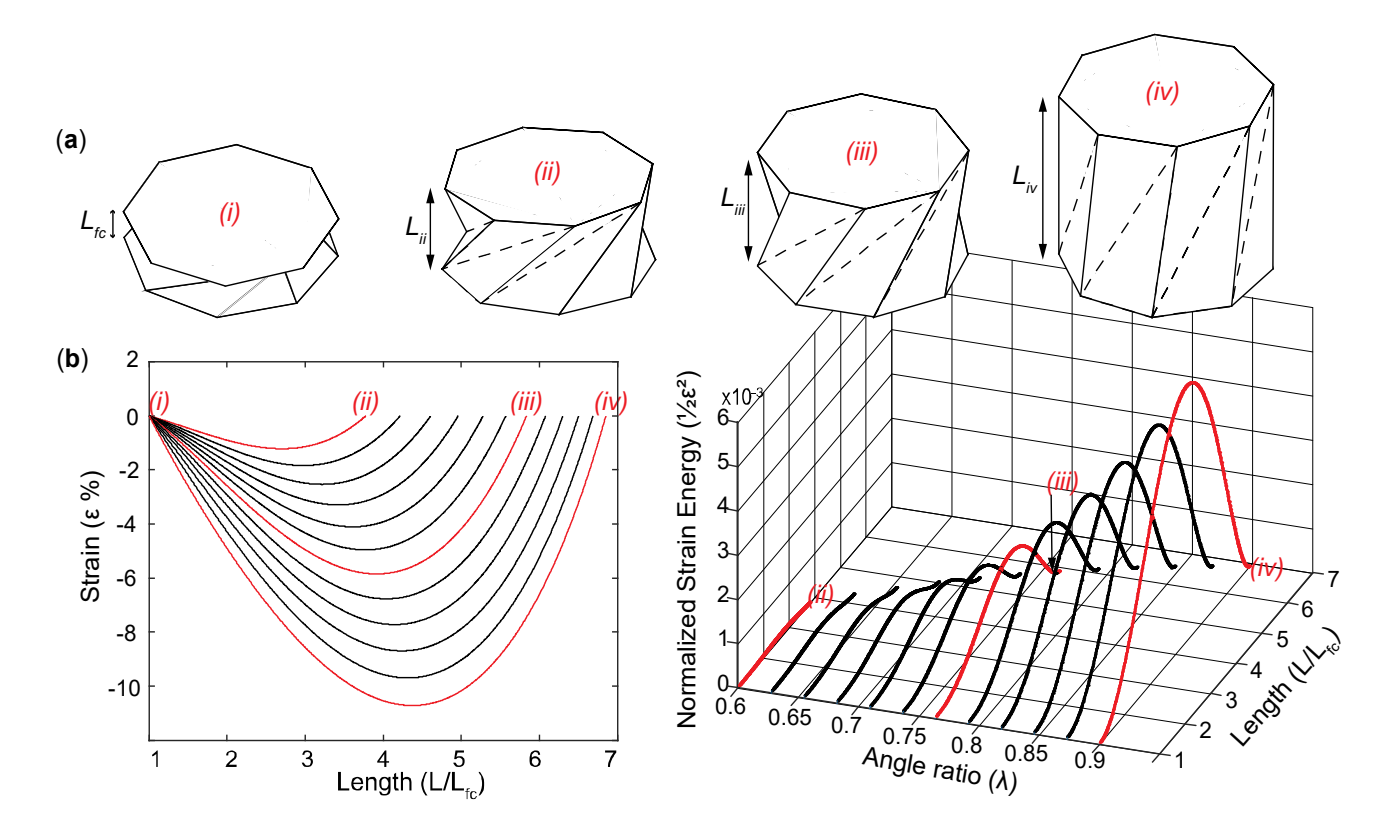


Figure 3: Generalized Kresling segment (a) The folding geometries of three different generalized Kresling segments that have the same length at fully-folded configuration (shown in (i)) but different lengths at fully-open configuration (shown in (ii), (iii), and (iv)). In this case, the angle ratio is different among these three segments, i.e. $\lambda_{ii} > \lambda_{ii} > \lambda_{ii}$

$$L = \left(L_{fc}^{2} + 2R^{2} \left(\cos\left(\alpha + 2\phi\right) - \cos\left(\alpha_{fc} + 2\phi\right)\right)\right)^{1/2}.$$
 (5)
$$E = \frac{1}{2}\varepsilon^{2}.$$

From the fully-folded geometry we can determine the upper limit for α to be, $\alpha_{fc} = 2\lambda_i \theta$. The lower limit for α can be computed by substituting Equation (5) in (6), which states that the length of the mountain crease is equal to b_g in fully-open and fully-folded configurations,

$$b_g = \left(2R^2\left(1 - \cos\left(\alpha\right)\right) + L^2\right)^{1/2} \text{ for } \alpha = \alpha_{fc} \text{ and } \alpha_{fo}.$$
 (6)

Thus, we have closed form solutions for describing the folding kinematics. Equations (4) and (5) can now be written in terms of the rotation angle ($\alpha_{fo} \le \alpha \le \alpha_{fc}$). The strain (ε) and strain energy (U) due to folding can now be calculated as,

$$\varepsilon = \frac{b - b_g}{b_o}$$
, and $U = \frac{1}{2}K\varepsilon^2$. (7)

Here, K is the material stiffness coefficient. For the purpose of this analysis we normalize the strain energy U by K, and define the non-dimensional strain energy as,

An origami mechanism is rigid foldable if all facets remain flat and rigid throughout the folding motion. On the other hand, if folding induces facet deformation, the origami is considered non-rigid foldable. The non-rigid foldability of cylindrical origami patterns like Kresling segment has been proven in literature [13,20]. The presence of bistability in a Kresling segment is due to the non-rigid foldable nature of the facets. That is, its facets are un-deformed at the two stable states, but they have to undergo some deformation while folding between the two stable states. The range of angle ratio for the bistability of Kresling segment is $0.5 < \lambda_g < 1$ [13]. Higher angle ratio (λ_g) corresponds to stronger bistability (Figure 3(b)). Kresling segments with same fully-folded length can be designed to have different fully-open lengths by changing the angle ratio as shown in Figure 3(a).

3. MULTI-STABLE MECHANISM USING GENERALIZED KRESLING SEGMENT

In this study, we use a chain of serially connected, generalized Kresling segments as a driving module to demonstrate the use of multi-stability for peristaltic gait generation. We relax the metameric (identical) segmentation requirement and allow the Kresling segments in a module to feature different angle ratios. We analyze the resulting multi-stable system and identify its paths of deformation under end displacement control. Such deformation paths are referred to as "equilibrium paths" hereafter. We also examine how each Kresling segment deforms along the equilibrium paths.

First, we describe how to identify the equilibrium paths of a Kresling based driving module. The potential energy landscape of such a multi-stable system lies on the (n+1)-dimensional hypersurface created by combining n-bistable segments. It can have a maximum of 2^n stable configurations [21]. The problem of computing the equilibrium path followed by a multi-stable driving module under displacement control can be formulated as an optimization problem to find the local potential energy minima corresponding to a prescribed total length [21,22]. The total potential energy (E_{total}) and total length (L_{total}) of a driving module are defined as,

$$E_{total} = \sum_{i=1}^{n} E_i(L_i), L_{total} = \sum_{i=1}^{n} L_i,$$
 (9)

where L_i is current length of the segment #i and E_i is corresponding potential energy. When the total length (L_{total}) of the system is prescribed, lengths of first n-1 segments $(L_1, L_2, \cdots, L_{n-1})$ can be specified as the minimizers and length of the last segment (L_n) can be calculated based on a constraint equation. Thus, the optimization problem can be described as follows:

Minimize
$$E_{total} = \sum_{i=1}^{n-1} E_i(L_i) + E_n(L_{total} - \sum_{i=1}^{n-1} L_i)$$
where $i = 1, 2 \dots n-1,$
subject to $L_n = L_{total} - \sum_{i=1}^{n-1} L_i,$

$$L_{\min i} \leq L_i \leq L_{\max i} \text{ and } L_{\min n} \leq L_n \leq L_{\max n}.$$
(10)

In other words, the input variable is the total length of driving module (L_{total}). It is varied from the minimum to the maximum value in incremental steps of ΔL_{total} as follows,

$$L_{total}^{\min} = \sum_{k=1}^{n} L_{\min k} \text{ , } L_{total}^{\max} = \sum_{k=1}^{n} L_{\max k} \text{ and } m = \frac{(L_{total}^{\max} - L_{total}^{\min})}{\Delta L_{total}},$$

where m is the total number of increments. For j^{th} iteration (=2...m), the output is defined as the vector of individual segment lengths $L^j = [L^j_1 \cdots L^j_{n-1}]$ corresponding to each L^j_{total} for which total energy of the system E^j_{total} is minimized according to the optimization problem defined in Equation(10). The following pseudo-code describes the optimization algorithm used:

<u>Step 1</u>: Initialize the optimization problem using initial stable configuration,

For segments i=1,2,...,n-1 define,

$$L_i^1 = L_{\min i}$$
 and $L_{total}^1 = L_{total}^{\min}$ for extension phase analysis, or $L_i^1 = L_{\max i}$ and $L_{total}^1 = L_{total}^{\max}$ for contraction phase analysis, where $L^1 = [L_1^1 \quad \cdots \quad L_{n-1}^1]$.

<u>Step 2</u>: Each increment step j (=2...m), corresponds to a unique total length of the driving module. Define,

$$\begin{split} L_{total}^{j} &= L_{total}^{j-1} + \Delta L_{total} \ for \ extension \ phase \ analysis, or \\ L_{total}^{j} &= L_{total}^{j-1} - \Delta L_{total} \ for \ contraction \ phase \ analysis, where \\ L_{0}^{j} &= [L_{1}^{j-1} \quad \cdots \quad L_{n-1}^{j-1}] = L^{j-1}. \end{split}$$

Here, L_{total}^{j} is the total length of driving module. L_{0}^{j} is the initial input specified to solve the optimization problem.

<u>Step 3</u>: Solve the optimization problem described in Equation(10). The initial input L_0^j is used as the first guess to find optimized lengths of the individual segments and corresponding total energy of the module,

$$L^{j} = [L_{1}^{j} \cdots L_{n-1}^{j}]$$
 and E_{total}^{min} ,

and the length of the last segment is written as,

$$L_n^j = L_{total}^j - \sum_{k=1}^{n-1} L_k^j.$$

<u>Step 4</u>: Set $L_0^{j+1} = [L_1^j \cdots L_{n-1}^j]$ i.e. the output vector of individual segment lengths in j^{th} iteration is provided as initial input for the next $j+I^{\text{th}}$ iteration.

<u>Step 5</u>: Set j=j+1. Repeat the process till j=m.

Note that the optimization algorithm above only gives one equilibrium path after each iteration, but multiple equilibrium paths are possible for a multistable system [22]. We can repeat the optimization process with different initial input variables to ensure all possible equilibrium paths are found. Once the equilibrium paths are identified, then corresponding force-deformation relationships can be obtained by differentiating the equilibrium energy-deformation path.

Now, we have enough background to analyze the multi-stability of a Kresling chain. For this work, we use a dual-segment driving module as a case study example. The aforementioned analysis method is applied to find the equilibrium paths followed by this dual-segment system, and corresponding design parameters are listed in Table 1.

Table 1: Parameters used for the Multi-stability analysis of Kresling based dual-segment driving module

Parameters	Segment-1	Segment -2
n	8	8
p (mm)	30	30
λ_i	0.8	0.6
L _{fc} (mm)	15	10

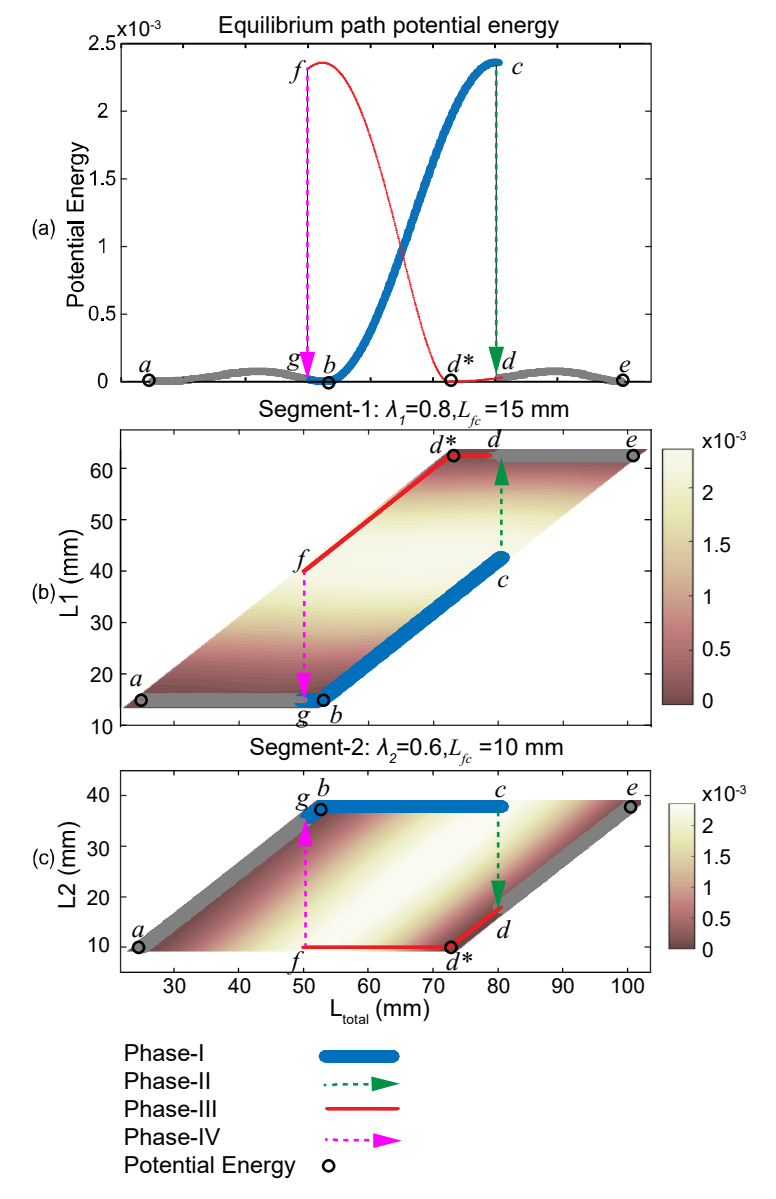


Figure 4: Multi-stability analysis results for the dual-segment driving module. The gray, blue and red curves represent the equilibrium path followed during the extension and contraction phases. (a) Potential energy along the equilibrium path of the extension and contraction phase. The energy minima are shown with black dots, (b) The segment-1 length change throughout the folding motion, (c) The segment-2 length change throughout the folding motion. The phases-I to IV of gait generation (discussed in section-4) are shown here for more clarity. The energy landscape for the multi-stable Kresling module is superimposed as the color map to the plots to show the total energy variation in different stages.

The results of the optimization algorithm applied to the Kresling based dual-segment driving module show two different equilibrium paths, each visiting three potential energy minima (Figure 4 (a)). The combined equilibrium paths describe the folding and unfolding deformation of two Kresling segments when

the *total length* is controlled as shown in Figure 4. When the total length of a Kresling based module is increased from its minimum value to the maximum (referred as "extension phase" hereafter), it will follow the path of $a \rightarrow b \rightarrow c \rightarrow d \rightarrow e$. On the other hand, if the total length is decreased from the maximum to minimum ("contraction phase"), the Kresling based module deforms by following $e \rightarrow d^* \rightarrow f \rightarrow g \rightarrow a$. We see two "jumps" between the equilibrium paths: one occurs during the extension phase $(c \rightarrow d)$ and the other occurs during the contraction phase $(f \rightarrow g)$. During these jumps, the two Kresling segments deform significantly, due to the rapid release of potential energy, without changing their total length. Such a phenomenon will be crucial for generating the peristaltic locomotion gait (as we detail in Section 4).

More importantly, we also examine how individual segment deforms (or folds) during the extension and contraction phase, particularly at the jumps between equilibrium paths. The equilibrium path followed by individual segments depends on their angle ratio λ_g . The segment with higher angle ratio will always follow path shown in Figure 4(b) and segment with lower angle ratio will always follow path shown in Figure 4(c). Without the loss of generality, we assume $\lambda_1 > \lambda_2$. If $\lambda_1 = \lambda_2$, we don't observe any discernible jumps so this case will not be discussed.

When $\lambda_1 > \lambda_2$, both jumps induce large length changes in the Kresling segments as shown in Figure 4(b,c). Accordingly, a cycle of full extension followed by a contraction phase can be divided into following six stages:

<u>Stage-I</u> $(a \rightarrow b)$: The dual-segment Kresling module extends from its fully-contracted state at point a. In this stage, the length of segment-1 remains near its minimum, while segment-2 length increases monotonically along $a \rightarrow b$ and reaches its maximum.

<u>Stage-II $(b \rightarrow c \rightarrow d)$ </u>: At the beginning of this stage, the segment-1 length starts to increases monotonically along $b \rightarrow c$, while the segment-2 length remains at its maximum. When the jump from c to d occurs, Segment-1 quickly unfolds to its maximum length at d, and segment-2 length decreases to a low value. Note that the total length of two segments remains unchanged during this jump.

Stage-III $(d \rightarrow e)$: For the rest of extension phase, segment-1 length remains at its maximum and segment-2 length increases monotonically till it reaches e. Therefore, at the end of this stage, both segments are in fully-extended state.

<u>Stage-IV ($e \rightarrow d^*$)</u>: In this stage, the dual-segment Kresling module starts to contract in its total length from e. The length of segment-1 remains near its maximum, while segment-2 length decreases monotonically along $e \rightarrow d^*$ and reaches its minimum.

<u>Stage-V $(d^* \rightarrow f \rightarrow g)$ </u>: Segment-1 length decreases monotonically along $d^* \rightarrow f$, while segment-2 length remains at its minimum. When the jump from f to g occurs, segment-1 quickly folds to minimum length configuration at g, and segment-2 length increases to near maximum.

Stage-VI $(g \rightarrow a)$: In this last stage of contraction, segment-1 length remains at minimum and segment-2 length decreases monotonically till it reaches a. At the end of this stage, both segments return to their fully-contracted state.

4. PERISTALTIC GAIT GENERATION

In this section, we propose the use of multi-stability described in Section 3 to generate the peristaltic locomotion gait. First of all, according to the retrograde peristalsis wave mechanism shown in Figure 1, some anchoring mechanism is required to keep the fully-contracted segments in place during locomotion. Such an anchoring function is typically achieved by expanding the segment radially when it is contracting in length. However, the Kresling segment itself does not contract or expand in its radial direction during unfolding and folding, so we need to implement some additional mechanism to fulfill the anchoring requirement. To this end, we take advantage of the folding kinematics of Kresling segment and propose an origami anchor (Figure 5). Such an anchor is attached to the creases of Kresling segment and it is

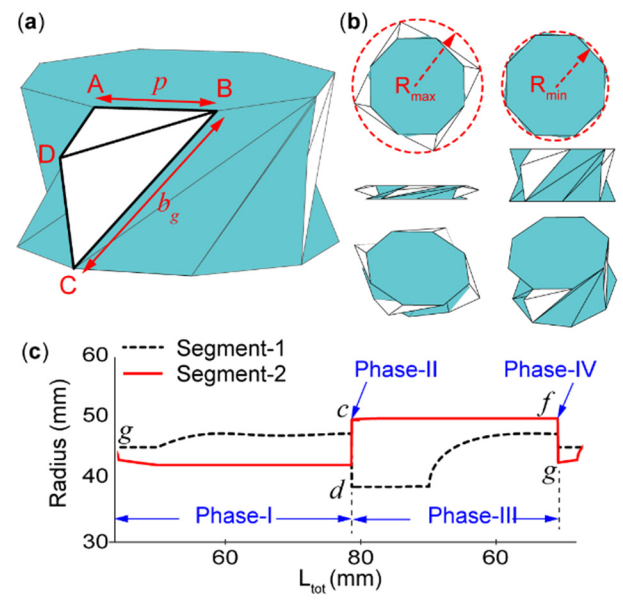


Figure 5: The origami anchoring element design (a) The anchoring element design parameters. (b) *To-scale* plot of the segment at fully-folded and fully-open stable states. (c) The anchoring element radius variation throughout the actuation cycle.

carefully designed to fold out (i.e. to increase the effective radius) while the Kresling segment contracts in length. This anchor is essentially two connected triangles that share a common side (ABD and CBD in Figure 5(a)). The side lengths $l_{\rm AB}=p$ and $l_{\rm BC}=b_g$, so that side AB can be glued to the side of polygonal base and side BC can be glued to the mountain crease of the Kresling. In this way, we can tweak the length of three other triangle sides, $l_{\rm AD}$, $l_{\rm BD}$ and $l_{\rm CD}$, according to several anchoring requirements as discussed below.

The first requirement is that only one Kresling segment in the driving module is anchored to the environment during any phase of the locomotion. To satisfy this, we designate a cutoff length: when the length of either Kresling segment is below this cutoff value, its anchors should be folded out enough to generate a contact with the surrounding environment. The cutoff length of segment-1 equals to its length at point c on its equilibrium path

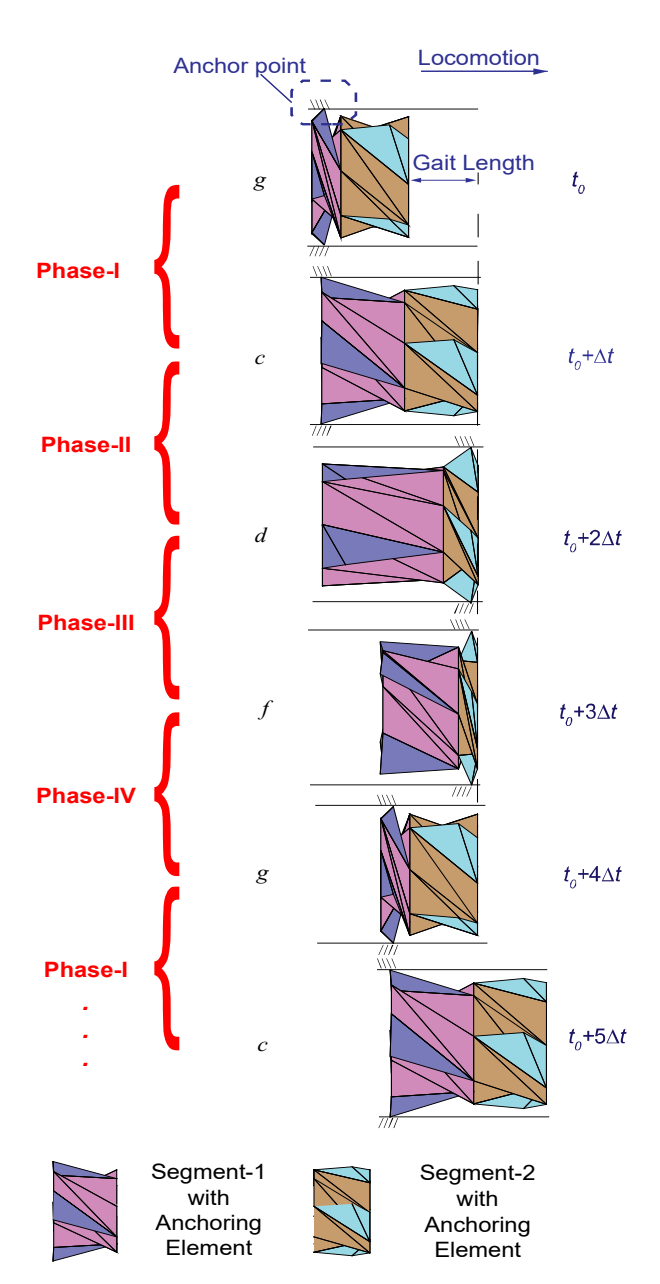


Figure 6: *To-scale* schematic diagram of the peristaltic locomotion gait generated by using the multi-stability of the dual-segment Kresling driving module.

shown in Figure 4(b), and cutoff length of segment-2 equals to its length at point d in Figure 4(c). The second requirement is that the origami anchor should fold without interfering with any of the Kresling segment facets. The third requirement is that the anchoring point D should only travel a small distance along the longitudinal direction of Kresling segment during folding. After several design iterations, the anchor designs are chosen as shown in Table 2.

Table 2: Origami anchor designs used in the case study

Parameters	Segment-1	Segment -2
I _{AD} (mm)	9.9	13.3
<i>I</i> _{BD} (mm)	29.8	41.5
Ico (mm)	48.8	25.0

With the help of the origami anchor, the peristaltic locomotion gait can be created by using the multi-stability of dual-segment Kresling module. Since only one segment should be anchored during locomotion, section $a \rightarrow g$ of the equilibrium paths shown in Figure 4 cannot be used otherwise both segments will be below their cutoff lengths (aka. both anchored). Section $d \rightarrow e$ of the equilibrium paths cannot be used either because both segments will be above their cutoff length (aka. both free). Therefore, we exploit the actuation cycle of $g \rightarrow c \rightarrow d \rightarrow f \rightarrow g$, and divide this cycle into 4 phases of effective locomotion as discussed below (Figure 4 and Figure 6):

<u>Phase-I</u> ($g\rightarrow c$): In this phase, the rear end of the segment-1 is anchored to the environment, and this segment is extending in length via unfolding. Meanwhile, segment-2 is extended at its near-maximum length. In this phase, the dual-segment module as a whole extends and moves forward.

<u>Phase-II (jump from c to d)</u>: During this phase, the Kresling module quickly jumps from point c of the equilibrium path to point d via releasing the stored potential energy. As a result, the anchor points switch from the rear end of segment-1 to the front end of segment-2. This is because during the jump, segment-1 quickly extends above its cutoff length, reaches its maximum length, and loses the anchoring. At the same time, segment-2 quickly contracts below its cutoff length, reaches near to its minimum length, and anchors to the environment. It is worth noting that during this rapid jump, the total length of the dual-segment does not change, thus the Kresling module overall stays at the same position, only the anchors are switched.

<u>Phase-III ($d \rightarrow f$)</u>: In this phase, the front end of the segment-2 remains anchored to the environment since this segment stays near its minimum length. While the segment-1 length decreases monotonically from its maximum, but without reaching the cutoff length. As a result, the module as whole contracts and continues to move forward.

<u>Phase-IV</u> (jump from *f* to *g*): During this jump, segment-1 quickly contracts near to its minimum length and anchors to the environment, while segment-2 extends quickly to its maximum lengths and loses the anchoring. As a result, the anchor points switch from the front end of the module back to its rear end, but the driving module overall stays at the same location.

After the second jump, the module is again at the start of Phase-I, so that the cycle of Phases-I to IV can be repeated to move the robot forward. The gait length can be approximated based on the deformation of two Kresling segments during Phases-I and III.

It is important to note that in this dual-segment driving module, we do not have a separate anchoring segment like in the earthworm shown in the Figure 1. Instead, we use the switching of anchor points during the jump at Phases-II and IV. Moreover, we do not actuate and control the segments individually like in the earthworm or other earthworm-inspired crawling robots. Instead, we only control the length of whole driving module, while the length of individual segments and the anchoring locations are "controlled" autonomously by the embedded multi-stability. This is an example of morphology assisted computation [23], which can significantly simplify the mechatronic system in a soft robot.

5. SUMMARY AND CONCLUSION

In this paper, we developed a unique approach of harnessing multi-stability for the crawling locomotion of earthworm-inspired, segmented soft robot. In particular, we showed that the elastic multi-stability embedded in an origami robot skeleton can be used to generate the *peristaltic gait*, and the required multi-stable mechanism can be created by serially combining bistable segments.

As a case study, we used *generalized Kresling segments* with different angle ratios, i.e. different bistability strengths, to create a dual-segment driving module of an earthworm inspired soft robot. Multi-stability analysis of this driving module revealed two jumps, one each in extension phase and contraction phase, which can induce rapid and large deformation of the two Kresling segments without changing their total length. We also proposed an origami based solution to fulfill the anchoring requirement. Finally, we combined the multi-stable Kresling based driving module with the anchoring elements to successfully generate peristaltic gait with a four-phase actuation cycle.

The results obtained from this case study can be used to design an origami based earthworm inspired soft robot. We have shown that, by carefully designing a multi-stable mechanism we can significantly reduce the number of actuators needed to control the robot. Also, we do not need a complex control architecture to individually manipulate each segment of the driving module. By simply controlling the length of the driving module as a whole and exploiting the embedded multi-stability, we can generate the peristaltic locomotion gait. Along with these benefits, we are also able to retain advantages of origami such as, self-packaging and compliance.

It is worth noting that the main focus of this work is to lay down the theoretical foundation for generating peristaltic gait using a multi-stable origami mechanism. The mechatronic design of the soft robot prototype, especially the mechanism for controlling the total module length, is beyond the scope of this work and will be taken up in the future. Currently, we are looking into motor-tendon system [12], pressurization, and SMA springs as possible candidates to control the length of the driving module.

In summary, this research developed an analytical method to actuate a dual-segment driving module. This approach can be further extended to a multi-segment driving module to generate more adaptable crawling locomotion gaits. Thus, a direct exploitation of multi-stability embedded in origami can significantly advance the state of art of crawling soft robot research by simplifying the mechanical and electrical design, reducing power requirement and decreasing overall mass of the robot.

6. ACKNOWLEDGEMENT

P. Bhovad and S. Li acknowledge the support by the National Science Foundation (Award # CMMI-1633952 and 1751449 CAREER) and the startup funding from Clemson University.

REFERENCES

- [1] Culha, U., Hughes, J., Rosendo, A., Giardina, F., and Calisti, M., 2017, *Soft Robotics: Trends, Applications and Challenges*, Springer International Publishing, Cham.
- [2] Laschi, C., Mazzolai, B., and Cianchetti, M., 2016, "Soft Robotics: Technologies and Systems Pushing the Boundaries of Robot Abilities," Sci. Robot., 1(1), p. eaah3690.
- [3] Quillin, K., 1999, "Kinematic Scaling of Locomotion by Hydrostatic Animals: Ontogeny of Peristaltic Crawling by the Earthworm Lumbricus Terrestris," J. Exp. Biol., **202** (Pt 6)(1999), pp. 661–74.
- [4] Fang, H., Wang, C., Li, S., Wang, K. W., and Xu, J., 2015, "A Comprehensive Study on the Locomotion Characteristics of a Metameric Earthworm-like Robot: Part B: Gait Analysis and Experiments," Multibody Syst. Dyn., **35**(2), pp. 153–177.
- [5] Ge, J. Z., Calderón, A. A., and Pérez-Arancibia, N. O., 2017, "An Earthworm-Inspired Soft Crawling Robot Controlled by Friction," arXiv Prepr., p. 1707.04084.
- [6] Seok, S., Onal, C. D., Cho, K. J., Wood, R. J., Rus, D., and Kim, S., 2013, "Meshworm: A Peristaltic Soft Robot with Antagonistic Nickel Titanium Coil Actuators," IEEE/ASME Trans. Mechatronics, 18(5), pp. 1485–1497.
- [7] Onal, C. D., Wood, R. J., and Rus, D., 2013, "An Origami-Inspired Approach to Worm Robots," IEEE/ASME Trans. Mechatronics, **18**(2), pp. 430–438.
- [8] Saga, N., and Nakamura, T., 2004, "Development of a Peristaltic Crawling Robot Using Magnetic Fluid on the Basis of the Locomotion Mechanism of the Earthworm," Smart Mater. Struct., **13**(3), pp. 566–569.
- [9] Horchler, A. D., Kandhari, A., Daltorio, K. A., Moses, K. C., Ryan, J. C., Stultz, K. A., Kanu, E. N., Andersen, K. B., Kershaw, J. A., Bachmann, R. J., Chiel, H. J., and Quinn, R. D., 2015, "Peristaltic Locomotion of a Modular Mesh-Based Worm Robot: Precision, Compliance, and Friction," Soft Robot., 2(4), pp. 135–145.
- [10] Lee, D.-Y., Kim, S.-R., Kim, J.-S., Park, J.-J., and Cho, K.-J., 2017, "Origami Wheel Transformer: A Variable-Diameter Wheel Drive Robot Using an Origami

- Structure," Soft Robot., **4**(2), pp. 163–180.
- [11] Marchese, A. D., Onal, C. D., and Rus, D., 2014, "Autonomous Soft Robotic Fish Capable of Escape Maneuvers Using Fluidic Elastomer Actuators," Soft Robot., 1(1), pp. 75–87.
- [12] Vander Hoff, E., Jeong, D., and Lee, K., 2014, "OrigamiBot-I: A Thread-Actuated Origami Robot for Manipulation and Locomotion," IEEE Int. Conf. Intell. Robot. Syst., (Iros), pp. 1421–1426.
- [13] Pagano, A., Yan, T., Chien, B., Wissa, A., and Tawfick, S., 2017, "A Crawling Robot Driven by Multi-Stable Origami," Smart Mater. Struct., **26**(9), p. 94007.
- [14] Fang, H., Zhang, Y., and Wang, K. W., 2017, "Origami-Based Earthworm-like Locomotion Robots," Bioinspiration and Biomimetics, **12**(6), p. 65003.
- [15] Miyashita, S., Guitron, S., Li, S., and Rus, D., 2017, "Robotic Metamorphosis by Origami Exoskeletons," Sci. Robot., **2**(10), p. eaao4369.
- [16] Kresling, B., 2008, "Natural Twist Buckling in Shells: From the Hawkmoth's Bellows to the Deployable Kresling-Pattern and Cylindrical Miuraori," Proc. 6th Int. Conf. Comput. Shell Spat. Struct., (May), pp. 1–4.
- [17] Guest, S. D., and Pellegrino, S., 1994, "The Folding of Triangulated Cylinders, Part I: Geometric Considerations," J. Appl. Mech., **61**(4), p. 773.
- [18] Hunt, G. W., and Ario, I., 2005, "Twist Buckling and the Foldable Cylinder: An Exercise in Origami," Int. J. Non. Linear. Mech., **40**(6), pp. 833–843.
- [19] Jianguo, C., Xiaowei, D., Ya, Z., Jian, F., and Yongming, T., 2015, "Bistable Behavior of the Cylindrical Origami Structure With Kresling Pattern," J. Mech. Des., 137(6), p. 61406.
- [20] Bös, F., Wardetzky, M., Vouga, E., and Gottesman, O., 2016, "On the Incompressibility of Cylindrical Origami Patterns," J. Mech. Des., **139**(2), p. 21404.
- [21] Oh, Y. S., and Kota, S., 2009, "Synthesis of Multistable Equilibrium Compliant Mechanisms Using Combinations of Bistable Mechanisms," J. Mech. Des., 131(2), p. 21002.
- [22] Overvelde, J. T. B., Kloek, T., D'haen, J. J. A., and Bertoldi, K., 2015, "Amplifying the Response of Soft Actuators by Harnessing Snap-through Instabilities," Proc. Natl. Acad. Sci., **112**(35), pp. 10863–10868.
- [23] Müller, V. C., and Hoffmann, M., 2017, "What Is Morphological Computation? On How the Body Contributes to Cognition and Control," Artif. Life, 23(1), pp. 1–24.